Planetary and Space Science 57 (2009) 78–82

Contents lists available at ScienceDirect

Planetary and Space Science

journal homepage: www.elsevier.com/locate/pss

Lunar Prospector measurements of secondary electron emission from lunar regolith

J.S. Halekas [a,*], G.T. Delory [a], R.P. Lin [a,b], T.J. Stubbs [c,d], W.M. Farrell [d]

[a] Space Sciences Laboratory, University of California, 7 Gauss Way, Berkeley, CA 94 720, USA
[b] Physics Department, University of California, Berkeley, CA, USA
[c] Goddard Earth Sciences and Technology Center, University of Maryland Baltimore County, Baltimore, MD, USA
[d] NASA Goddard Spaceflight Center, Greenbelt, MD, USA

ARTICLE INFO

Article history:
Received 15 July 2008
Received in revised form
24 November 2008
Accepted 25 November 2008
Available online 6 December 2008

Keywords:
Moon
Surface charging
Secondary electron emission
Lunar Prospector

ABSTRACT

We present the first in situ measurements of the secondary electron emission efficiency of lunar regolith, utilizing Lunar Prospector measurements of secondary electrons emitted from the negatively charged night side and accelerated upward by surface electric fields. By comparing measurements of secondary currents emitted from the surface and incident primary electron currents, we find that the secondary yield of lunar regolith is a factor of ~3 lower than that measured for samples in the laboratory. This lower yield significantly affects current balance at the lunar surface and the resulting equilibrium surface potentials. This information must be folded into models of the near-surface plasma sheath, in order to predict the effects on dust and other components of the lunar environment, and ultimately determine the importance for surface exploration and scientific investigations on the Moon.

1. Introduction

Like any object in space, the lunar surface charges in response to incident currents, reaching a floating potential with respect to the surrounding plasma such that positive and negative currents to the surface balance (Whipple, 1981). The currents to an object in space include those from charged particles in the surrounding plasma, independent of material properties. Typically, currents from lighter and faster electrons dominate over ion currents, acting to drive the surface negative. However, photoelectron and secondary electron emission currents, which depend on material and surface properties, also significantly affect the charging balance and the equilibrium potential. In sunlight, photoemission usually dominates, leading to a small positive potential. In shadow, depending on the secondary electron yield, surfaces can float either positive or negative. Indeed, early predictions of nightside lunar surface potentials ranged from near zero to −1800 V, for different assumed regolith secondary emission (Knott, 1973). Secondary electron emission from lunar materials has been measured in the laboratory, but not in situ.

The charging of the lunar surface has both scientific and practical interest. Charging of surfaces in space represents a fundamental physical process, worthy of study in its own right. In addition, near-surface electric fields resulting from surface charging strongly affect the plasma environment near the surface, as well as possibly significantly affecting the motion of lunar dust and ionized exospheric gases. Electric fields and dust near the surface may have important practical implications for robotic and human lunar exploration, as well as scientific observations from the surface (Stubbs et al., 2007). In order to understand and predict the charging characteristics of the surface, and the effects of lunar electric fields on dust and other components of the environment, we need in situ measurements of secondary electron yields from lunar regolith. To this end, we now present direct measurements of secondary electrons by Lunar Prospector (LP), and the resulting constraints on lunar secondary yields.

2. Methods

LP, which orbited the Moon in 1998–1999, included an Electron Reflectometer (ER) and a magnetometer (MAG). The ER provided 3-d electron data from ~7–40 eV (adjustable) to ~20 keV. This paper focuses on data from times when the Moon passed through the terrestrial magnetosphere in 1999, when the ER energy sweep reached the lowest energies (lowest energy bin centered at ~7 eV), allowing the best measurements of secondary electrons.

The ER was designed to measure the distribution of electrons adiabatically reflected from lunar crustal magnetic fields, thereby determining their magnitude; however, the reflectometry technique also proved capable of measuring electrostatic potential

* Corresponding author. Tel.: +1 510 643 4310; fax: +1 510 643 8302.
E-mail address: jazzman@ssl.berkeley.edu (J.S. Halekas).

0032-0633/$ - see front matter © 2008 Elsevier Ltd. All rights reserved.
doi:10.1016/j.pss.2008.11.009

differences between the surface and the spacecraft (Halekas et al., 2002). In addition, the ER measured secondary electrons produced at the surface and accelerated up to the spacecraft through these potential drops (Halekas et al., 2002). Both of these measurements provided diagnostics of the presence of significant negative lunar surface potentials (occasionally reaching kilovolt values) particularly in the terrestrial plasmasheet (Halekas et al., 2005). However, without spacecraft potential data, quantitative measurements were at first impossible. Therefore, we recently developed new techniques to estimate the LP spacecraft potential, allowing the first quantitative measurements from orbit of lunar surface potentials and the incident electrons which, in part, drive surface charging (Halekas et al., 2008). We now show that these techniques also allow the first in situ measurements of the secondary electron emission efficiency of lunar regolith. In order to measure the secondary electron emission efficiency, we must accurately measure both the electron flux incident on the surface, and the secondary flux from the surface. The latter does not require us to know the LP spacecraft potential or the surface potential, but for the former knowledge of both quantities proves critical.

Measuring secondary electrons from the lunar surface proves conceptually simple. Parallel electric fields accelerate secondary electrons (generated at initial energies of a few eV (Whipple, 1981)) along magnetic field lines up to the spacecraft, forming a field-aligned beam of electrons, with a center energy (measured at the spacecraft) corresponding to the potential difference between surface and spacecraft. We show a typical electron distribution measured above the lunar night side in Fig. 1. The combination of magnetic and electric fields below the spacecraft acts to reflect much of the incident electron population. However, the reflected flux at energy E and pitch angle $180-\alpha$ cannot exceed the incident flux at energy E and pitch angle α, assuming no net acceleration/deceleration of electrons during their round trip between the spacecraft and the reflection point (i.e. assuming adiabatic behavior, generally a good approximation). Therefore, upward-going flux that significantly exceeds the corresponding downward-going flux, as shown by the contours in Fig. 1, indicates a secondary electron population. The beam contains the great majority of the secondary flux (as determined by a straightforward integration), but some secondary flux also scatters to other (mostly nearby) pitch angles and energies, possibly indicating the effects of beam-plasma instabilities.

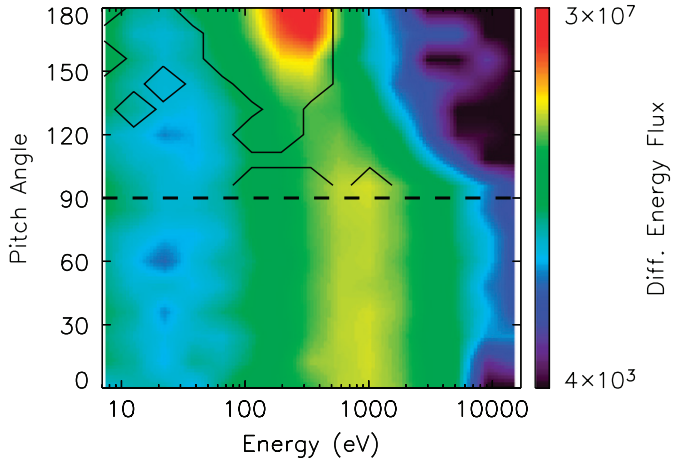

Fig. 1. Electron differential energy flux in eV/(cm^2 sr s eV) measured at 20:10:31 UT on April 29, 1999, with downward-going electrons at pitch angles $<90^\circ$, and upward-going electrons at pitch angles $>90^\circ$. Contours outline regions where upward flux exceeds corresponding downward flux by >2.5 standard deviations, indicating the presence of a significant secondary electron population in addition to adiabatically reflected primary electrons. The "loss cone" region of low upward-going flux above $\sim$1 keV indicates an electron population lost to the surface.

Our measurement of the total secondary electron current J_{SEC} does not depend on the potential of the surface U_M or the spacecraft U_{LP}, provided that all secondary electrons escape the near-surface region and reach the spacecraft. This requires a monotonic potential variation above the surface, and a large enough negative surface potential such that the beam (with a center energy of $-U_M$) can overcome any potential barrier at the spacecraft and arrive with sufficient energy for us to measure it, i.e. $(U_M–U_{LP})<\sim$10 V. We assume that the first requirement is satisfied. Though some authors have suggested non-monotonic potential variation above the dayside surface, to our knowledge no one has predicted non-monotonic potential variation on the night side. Meanwhile, we can confirm the second requirement observationally, and find that it is often satisfied on the lunar night side, allowing us to routinely measure secondary electrons in shadow. However, in order to determine the secondary emission yield, we also need to know the primary current to the surface, which requires quantitative measurements of plasma electron fluxes and lunar surface electrostatic potentials. We can now calculate these quantities using the methods of Halekas et al. (2008).

In order to calculate the primary electron current incident on the surface, we determine the downward-going electron flux at the spacecraft, and utilize measurements of the lunar surface potential to determine the amount of flux reaching the surface. To adequately represent the full downward-going electron distribution, we fit the measured spectrum, after correcting for spacecraft potential (as described by Halekas et al., 2008), to a kappa distribution of the form:

$$f(v)=\frac{\Gamma(\kappa+1)}{(\pi\kappa)^{3/2}\Gamma(\kappa-1/2)}\frac{n_0}{\Theta^3}[1+v^2/(\kappa\Theta^2)]^{-\kappa-1} \quad (1)$$

For this distribution, n_0 represents the density, κ the kappa index, and the temperature $T_0=\kappa/(\kappa–3/2)^*m\Theta^2/(2k)$, where Θ is the thermal velocity. From this distribution, we can calculate the total current incident on the lunar surface, integrating to find the formula:

$$J_0=n_0 q\sqrt{\frac{kT_0}{2\pi m}}\frac{\sqrt{\kappa-3/2}\Gamma(\kappa-1)}{\Gamma(\kappa-1/2)} \quad (2)$$

In fitting to the measured electron distribution to determine the quantities in Eqs. (1) and (2), we self-consistently took into account the spacecraft potential (see Halekas et al., 2008). However, we have not yet taken lunar surface charging into account, so we can only use Eq. (2) as is if the surface lies at zero potential with respect to the plasma. Our observations show that the nightside surface usually floats at a negative potential—therefore repelling electrons and preventing those at low energies from reaching the surface. By shifting the distribution in energy according to the lunar surface potential, and re-calculating the moments with the correct limits, one can show that this changes the density, temperature, and current of the electron population reaching the surface as follows:

$$n=n_0\left(1+\frac{qU_M}{(\kappa-3/2)kT_0}\right)^{1/2-\kappa} \quad (3)$$

$$T=T_0\left(1+\frac{qU_M}{(\kappa-3/2)kT_0}\right) \quad (4)$$

$$J=J_0\left(1+\frac{qU_M}{(\kappa-3/2)kT_0}\right)^{1-\kappa} \quad (5)$$

In Fig. 2, we show LP ER data from a typical series of orbits around the Moon in the terrestrial magnetosphere. We determine

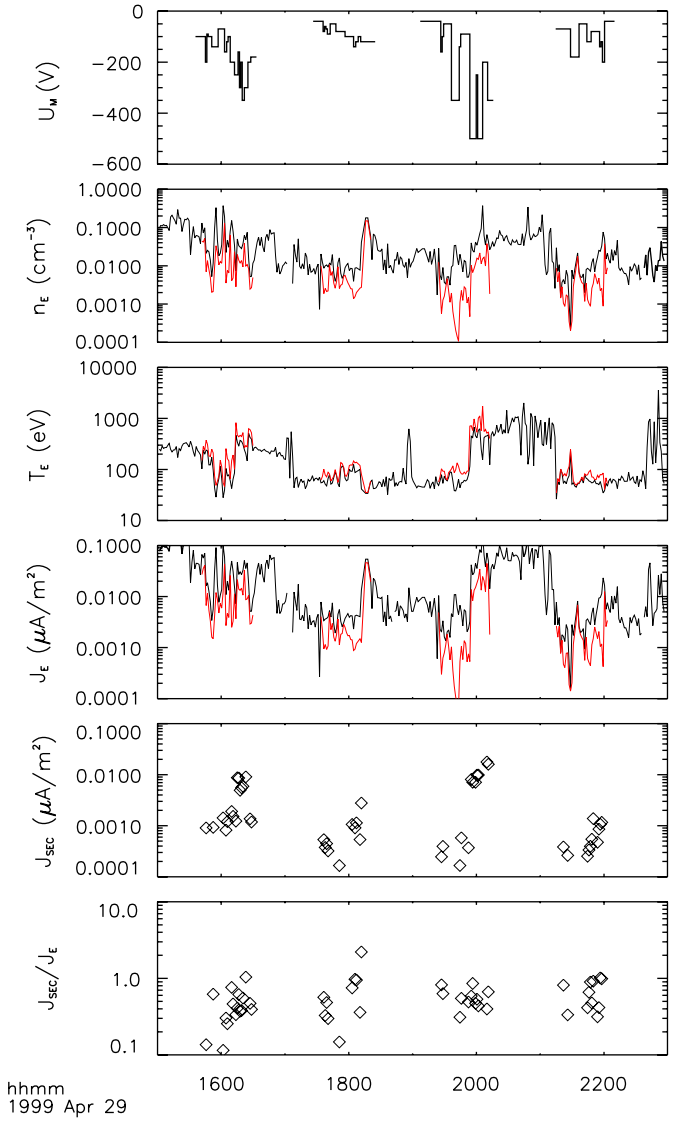

Fig. 2. Top panel shows lunar surface potential U_M on the night side. Next three panels show measurements of downward-going electron density n_E, temperature T_E, and current J_E at spacecraft altitude (black) and inferred values at the surface (red, night side only). Final two panels show secondary electron current J_{SEC} and the ratio of secondary electron current to incident electron current J_{SEC}/J_E at the surface, for times when we observe a clear population of secondary electrons. (For interpretation of the references to color in this figure legend, the reader is referred to the web version of this article.)

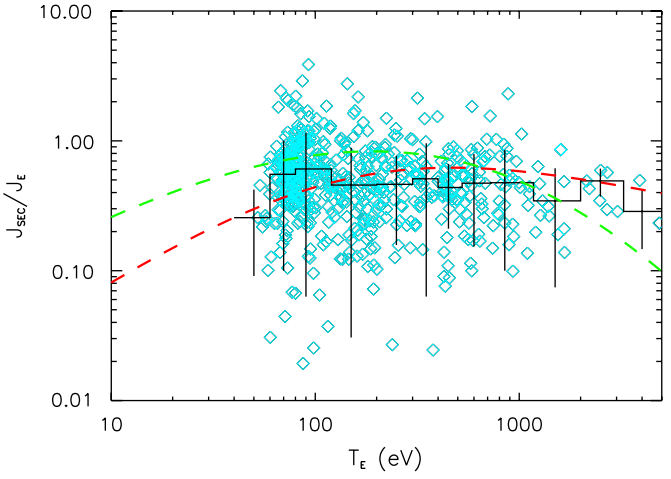

Fig. 3. Ratio of secondary electron emission current to incident electron current at the surface as a function of electron temperature at the surface. Median values and standard deviations shown in black. Best fit secondary emission models shown for Sternglass formula (green, $\delta_M^{eff} = 1.0$, $E_M = 350$ eV) and Katz formula (red, $\delta_M = 0.5$, $E_M = 350$ eV). (For interpretation of the references to color in this figure legend, the reader is referred to the web version of this article.)

downward-going electron properties by using kappa fits (Eq. (1)) to the downward-going electron spectrum at the spacecraft (corrected for spacecraft potential). We then infer the electron properties at the nightside surface by using Eqs. (3)–(5), taking into account the measured surface potential (using the methodology of Halekas et al., 2008). At the surface, we expect a higher electron temperature, and lower density and current, because of the velocity filtration of a non-Maxwellian distribution by the retarding negative nightside surface potential. All electron quantities, including the current to the surface, vary over orders of magnitude in the terrestrial magnetosphere, as the Moon passes through the lower temperature tail lobes and the higher temperature plasmasheet.

Meanwhile, utilizing the direct integration of secondary electron fluxes described above, we calculate the total secondary electron current from the surface. Note that the measurement of secondary electron current is completely independent from that of incident (primary) electron current, utilizing completely different parts of the electron distribution. Nonetheless, for most time periods J_E and J_{SEC} correlate with a rank correlation coefficient $R > 0.8$, indicating a fairly direct relation between primary and secondary current, as expected. We find the ratio J_{SEC}/J_E close to ~0.5, but with significant scatter, as shown in Fig. 3. We note that one does not in general expect the primary and secondary currents to balance (i.e. $J_{SEC}/J_E \neq 1$), since ions also contribute to the current balance at the surface.

If the surface potential was not in equilibrium with the surrounding plasma, this could affect our analysis. However, one can show that this situation is unlikely by considering the charging/discharging time-scale of the lunar surface. The nightside surface charge density is on the order of 10^{-12} C/m^2 for the potentials, densities, and temperatures observed in this study (we can calculate the surface charge density from $\sigma = \varepsilon_0 E$, and so assuming simple Debye shielding, $\sigma = \varepsilon_0 E \sim \varepsilon_0 U_M/\lambda_D$). Given the measured currents, this ensures that the time-scale for the surface to equilibrate with the plasma should be only a small fraction of a second. Therefore, we consider our measured values of J_{SEC}/J_E reliable and robust.

3. Results

Utilizing the methodology described above, we calculate J_{SEC}/J_E for all orbits over the lunar night side in the terrestrial magnetosphere in 1999 when the energy sweep extended down to 7 eV. For all times when we orbited over regions with no strong crustal magnetic fields, and observed a clear secondary beam, we plot this ratio as a function of electron temperature at the surface (as determined from Eq. (4)) in Fig. 3.

We can express the current ratio, equal to the integrated secondary yield, as

$$\delta = \frac{J_{SEC}}{J_E} = \frac{1}{J_E}\int \frac{dJ_E}{dE}\delta(E)\,dE \quad (6)$$

In this equation (with all quantities evaluated at the surface), the differential flux dJ_E/dE is easily related to $f(v)$, allowing a calculation of the expected secondary yield from a given electron distribution (using fits to the functional form of Eq. (1)) if we know the form of the secondary yield $\delta(E)$. Because of the

normalization, the total secondary yield depends only on the temperature at the surface T_E and the κ parameter, with only a weak dependence on κ. We use an average $\kappa = 4.5$ for all secondary yield predictions, and vary T_E. We consider two commonly used models for secondary emission. We first consider the Sternglass formula $\delta(E) = 7.4\delta_M(E/E_M)\exp(-\sqrt{(E/E_M)})$ (Sternglass, 1954), valid for normal incidence on a surface, but also usable for isotropic incidence (suitable for plasma electrons incident on the lunar surface), by replacing δ_M with $\delta_M^{eff} = 2\delta_M$ (Horányi et al., 1998). Here, δ_M is the peak yield, and E_M is the energy of the peak. We also consider the Katz formula, a more complicated formula that takes into account the angular dependence of the yield (Katz et al., 1977; Whipple, 1981). We plot secondary yield predictions (assuming isotropic incidence) using both of these formulae in Fig. 3, for comparison with the measured results. We find that our measurements roughly match predicted yields for $\delta_M = 0.5$, or $\delta_M^{eff} = 1.0$. In the temperature range covered by our measurements, we cannot clearly distinguish between the Katz and Sternglass models, though our data more closely match the Katz model. Unfortunately, for $T_E < \sim 50$ eV, where the two models diverge most significantly, the lunar surface does not charge to large enough negative potentials to produce a secondary beam measurable at the spacecraft.

Our data (though they constrain δ_M more strongly than E_M) are consistent with E_M of ~300–700 eV, as measured in the laboratory (Horányi et al., 1998; Willis et al., 1973). On the other hand, our data indicate lower peak yields (by a factor of ~3) than those experiments, which both found approximate values of $\delta_M = 1.5$, or $\delta_M^{eff} = 3.0$. Both experiments used electron beams, resulting in a measurement of the yield for normal incidence. Willis et al. (1973) performed experiments on a bulk sample, while Horányi et al. (1998) used single dust grains. Nevertheless, these experimenters reported similar results, with yields ~3 times higher than those implied by LP measurements. The discrepancy between our observations and the laboratory measurements may result from the roughness of the lunar regolith, which likely affects the escape of secondary electrons from the surface.

The scatter in the secondary yield from our measurements reflects a high degree of variability and/or experimental error. We considered the possibility that this variability reflects compositional effects, but we could not discern systematic differences in secondary emission from different lunar geologic units. Alternatively, some of the variability in secondary electron yield could result from secondary electrons from ion impact, though these should prove much less important than those from electron impact. Finally, some of the scatter could result from variability in surface roughness or other properties of the local regolith.

If we instead assume that the entire scatter in the distribution results from experimental error (difficult to estimate a priori), we can arrive at a worst-case estimate of this error. To this end, we plot the frequency distribution of all integrated secondary yield measurements (since we observe little energy variation over the measurement range, we consider all energies simultaneously) in Fig. 4. We find a distribution of integrated secondary yield, which other than a long tail at high values, is essentially normal. This distribution is centered at ~0.45, with a FWHM of 0.64. We emphasize that some of this scatter may reflect real differences in secondary emission yields from different regions of the lunar regolith. However, even in the worst case, if all scatter results from experimental error, we can estimate an integrated secondary yield of 0.45 ± 0.32. We cannot directly relate this value to a δ_M, since it represents an integrated value. However, Fig. 3 shows that it corresponds approximately to $\delta_M = 0.5$, or $\delta_M^{eff} = 1.0$, ~3 times lower than laboratory results. Even with worst-case errors, this value remains clearly lower than those reported in the laboratory, with important consequences for lunar surface charging. We cannot similarly test for systematic errors, which may also occur. However, we expect them to prove less important, especially given the consistency check presented next.

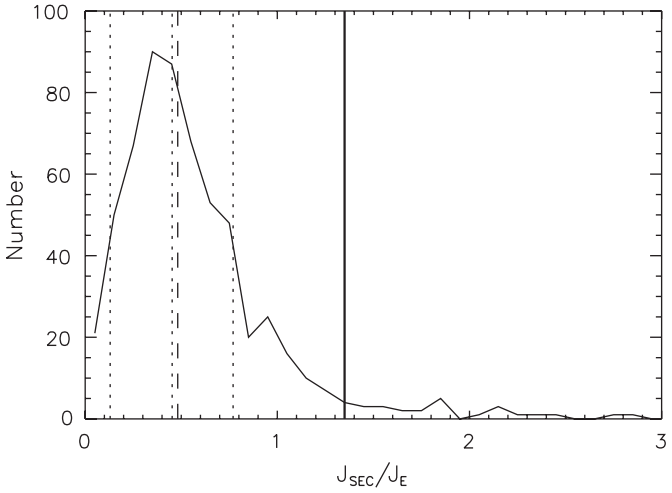

Fig. 4. Frequency distribution of ratio of secondary electron emission current to incident electron current at the surface. Dashed line shows median of distribution (0.48). Dotted lines show the limits and center of the full-width at half-maximum of distribution (FWHM = 0.64, center = 0.45). Thick solid vertical line shows value approximately consistent with laboratory measurements.

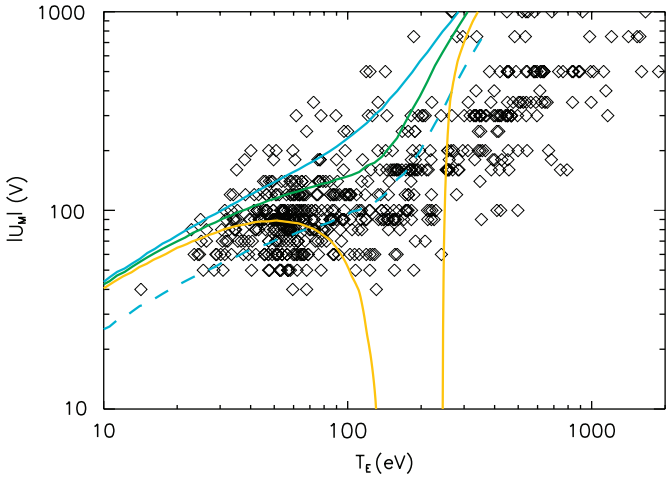

Fig. 5. Magnitude of negative nightside lunar surface potential as a function of electron temperature. Representative predictions are shown for modeled surface charging given secondary emission from Sternglass formula with $\delta_M^{eff} = 1.0$ (blue), 1.1 (green), and 1.2 (orange), with $T_I = T_E$. Dashed blue line shows corresponding model for $\delta_M^{eff} = 1.0$, but with $T_I = 10^* T_E$. (For interpretation of the references to color in this figure legend, the reader is referred to the web version of this article.)

4. Simple charging model

As a final exercise, we investigate whether our measured secondary yields prove consistent with the measured dependence of nightside surface potentials on electron temperature. To this end, we plot the magnitude of the measured negative nightside surface potential as a function of electron temperature in Fig. 5, along with representative predictions. We calculate predicted surface potentials utilizing a simple surface-charging model in which we assume ion temperature and density equal to the electron temperature and density, and secondary emission for a variety of different models. We then integrate the fluxes of each species to/from the surface as a function of surface potential,

thereby determining the surface potential at which the currents from ions, electrons, and secondary electrons balance (as in Halekas et al., 2008). We find that secondary emission models consistent with our secondary yield data over-predict the surface potential. We must emphasize that, given the simplicity of our charging model, which characterizes the electron distribution with a single temperature and assumes an ion distribution, the poor fit to observations is unsurprising. However, increasing the effective peak secondary yield from 1.0 to 1.2 in our model produces a qualitatively different predicted potential dependence on temperature, with higher secondary emission acting to prevent negative surface charging and produce near zero surface potentials for a range of electron temperatures near the peak in the secondary yield. This behavior is independent of the details of the charging model—any time the secondary yield exceeds unity, the surface must charge positive instead of negative. Our measurements of surface potentials, which remain negative over the full range of temperatures, therefore strongly rule out secondary emission models with higher peak yields. Our charging model assumes equal ion and electron temperatures; in fact, ion temperature may significantly exceed electron temperature in this region of the terrestrial magnetosphere. When we fold this into our charging model, we predict surface potentials much more in line with measurements, though still somewhat too large at high electron temperatures. Other improvements to the charging model should further improve the agreement with observations.

In any case, though our simple charging model cannot yet fully reproduce the charging data, the measured surface potentials—and the fact that they remain negative over the whole temperature range—clearly imply a lower secondary yield from lunar regolith in situ than that measured in the laboratory, consistent with the direct measurements of the secondary emission efficiency presented in this paper.

5. Conclusions

Using LP ER data, we directly measure secondary electrons emitted from the lunar surface. Utilizing recently developed techniques, we can also estimate the electron current incident on the lunar surface. From these two quantities, we derive the integrated secondary electron emission efficiency as a function of electron temperature. We find that the secondary electron yield from lunar regolith in situ is a factor of ~3 smaller than that measured in the laboratory. We suggest that this discrepancy may result at least partly from surface roughness effects, since low-energy secondary electrons cannot as easily leave the uneven lunar surface regolith without a collision. Alternatively, some type of non-equilibrium behavior, non-monotonic potential structure, or additional current source could perhaps explain the discrepancy. However, given the rapid surface-charging time-scales and the consistency in our observations of surface potentials and primary and secondary currents, we favor the former explanation.

Whatever the cause, smaller secondary yields have fundamental implications for lunar surface charging, allowing the night side to charge negative for a wider range of electron temperatures. These smaller secondary yields therefore must be folded into models of the plasma sheath near the lunar surface, in order to predict the effects on dust and other components of the lunar environment, and ultimately determine the importance for surface exploration and scientific investigations on and from the lunar surface.

Acknowledgement

This work was supported by the NASA grants NNG06GJ23G and NNX07AG10G.

References

Halekas, J.S., Mitchell, D.L., Lin, R.P., Hood, L.L., Acuña, M.H., 2002. Evidence for negative charging of the lunar surface in shadow. Geophys. Res. Lett. 29.

Halekas, J.S., Lin, R.P., Mitchell, D.L., 2005. Large negative lunar surface potentials in sunlight and shadow. Geophys. Res. Lett. 32, L09102.

Halekas, J.S., Delory, G.T., Lin, R.P., Stubbs, T.J., Farrell, W.M., 2008. Lunar Prospector observations of the electrostatic potential of the lunar surface and its response to incident currents. J. Geophys. Res. 113, A09102.

Horányi, M., Walch, B., Robertson, S., Alexander, D., 1998. Electrostatic charging properties of Apollo 17 lunar dust. J. Geophys. Res. 103, 8575–8580.

Katz, I., Parks, D.E., Mandell, M.J., Harvey, J.M., Brownell, D.H., Wang, S.S., Rotenberg, M., 1977. A three dimensional dynamic study of electrostatic charging in materials. NASA CR-135256.

Knott, K., 1973. Electrostatic charging of the lunar surface and possible consequences. J. Geophys. Res. 78, 3172–3175.

Sternglass, E.J., 1954. The Theory of Secondary Emission, Sci. Pap., 1772. Westinghouse Res. Lab., Pittsburgh, PA.

Stubbs, T.J., Vondrak, R.R., Farrell, W.M., 2007. Impact of dust on lunar exploration. In: Krüger, H., Graps, A.L. (Eds.), Dust in Planetary Systems, Workshop, September 26–30, 2005, Kauai, HI, Sp-643. ESA Publications, pp. 239–244.

Whipple, E.C., 1981. Potentials of surfaces in space. Rep. Prog. Phys. 44, 1197–1250.

Willis, R.F., Anderegg, M., Feuerbacher, B., Fitton, B., 1973. Photoemission and secondary electron emission from lunar surface material. In: Grard, R.J.L., Reidel, D. (Eds.), Photon and Particle Interactions with Surfaces in Space. Dordrecht, Netherlands, pp. 389–401.